

# Petal-Graphyne: A Novel 2D Carbon Allotrope for High-Performance Li and Na Ion Storage

Kleuton A. L. Lima<sup>a</sup>, José A. S. Laranjeira<sup>b</sup>, Nicolas F. Martins<sup>b</sup>, Alexandre C. Dias<sup>c,d</sup>, Julio R. Sambrano<sup>b</sup>, Douglas S. Galvão<sup>a</sup> and Luiz A. Ribeiro Junior<sup>c,e,\*</sup>

<sup>a</sup>Department of Applied Physics and Center for Computational Engineering and Sciences, State University of Campinas, Campinas, 13083-859, SP, Brazil

<sup>b</sup>Modeling and Molecular Simulation Group, São Paulo State University (UNESP), School of Sciences, Bauru, 17033-360, SP, Brazil

<sup>c</sup>Institute of Physics, University of Brasília, Brasília, 70910-900, DF, Brazil

<sup>d</sup>International Center of Physics, University of Brasília, Brasília, 70910-900, DF, Brazil

<sup>e</sup>Computational Materials Laboratory, LCCMat, Institute of Physics, University of Brasília, Brasília, 70910-900, DF, Brazil

## ARTICLE INFO

### Keywords:

Petal-Graphyne  
2D carbon allotrope  
DFT  
Energy storage  
Lithium-ion batteries  
Sodium-ion batteries

## ABSTRACT

Using density functional theory simulations, this study introduces Petal-Graphyne (PLG), a novel multi-ring metallic structure composed of 4-, 8-, 10-, and 16-membered rings. Its structural, electronic, and lithium/sodium storage properties were comprehensively investigated. PLG exhibits a high theoretical capacity of 1004 mAh/g for Li, Na, and mixed-Li/Na-ions, surpassing conventional graphite anodes. The material remains metallic, with multiple band crossings at the Fermi level. The optimal energy barriers for Li (0.28 eV) and Na (0.25 eV) on PLG and favorable diffusion coefficients in both monolayer and multilayer configurations are unveiled. The open circuit voltages are 0.47 V for Li, 0.51 V for Na, and 0.54 V for mixed-ion storage, suggesting stable electrochemical performance. These results highlight PLG as a promising candidate for next-generation lithium and sodium-ion batteries, combining high storage capacity and efficient ion transport.

## 1. Introduction

Two-dimensional (2D) carbon allotropes have been extensively studied due to their exceptional structural and electronic properties, which makes them attractive for a variety of applications, such as in energy storage, catalysis, and nanoelectronics [1–3]. Among these materials, porous 2D carbon allotropes are of particular interest as they present high surface area-to-volume ratio and tunable electronic properties, which are important for efficient ion transport in battery applications [4, 5]. Multi-membered rings in such structures can enhance ion diffusion and provide diverse adsorption sites, enhancing their performance in energy storage devices [4, 6, 7].

Computational studies, particularly density functional theory (DFT)-based simulations, play a key role in reliably predicting new 2D materials and assessing their stability, electronic properties, and electrochemical performance before experimental realization [8–11]. Examples of already obtained 2D carbon allotropes include graphene [12], graphyne [13], biphenylene [14], and monolayer fullerene networks [15–19]. Other examples of predicted/proposed structures are Penta-graphene [20], Popgraphene [21], Phagraphene [22], Irida-graphene [23], Sun-graphyne [24], and PolyPyGy [8], which highlights the diversity of possible carbon allotropes.

Many 2D carbon allotropes exhibit low conductivity or suboptimal ion diffusion, limiting their performance in lithium and sodium-ion batteries (LIBs and SIBs) [25]. In this way, there is a renewed interest in designing new structures that could overcome these limitations, which require

intrinsic metallicity, ensuring efficient charge transport, and offering potential high storage capacities. As an example, high diffusion rates and good storage capacities have been reported for Li and Na ions on materials such as biphenylene network [26, 27], Irida-graphene [10, 11], TODD-graphene [28], Tolanene [29], and TPDH-graphene [30], as well as other related 2D porous carbon materials [31–34].

Inspired by these results, here we proposed a new 2D carbon allotrope named petal-Graphyne (PLG) (Fig. 1). PLG has a unique combination of sp and sp<sup>2</sup> hybridization, featuring 4-, 8-, 10-, and 16-membered rings designed for high-capacity lithium and sodium-ion storage. Based on the recent experimental advancements in the on-surface synthesis of cyclocarbons structures [35], the PLG synthetic feasibility is within our present capabilities and could be, in principle, achieved via retro-Bergman ring-opening reactions from molecular precursors containing 4-, 8-, 10-, and 16-membered rings, which are structural motif also present in PLG.

In this work, we have carried out a comprehensive DFT-based study on the structural, electronic, and electrochemical PLG properties. Our results show that PLG has metallic and good lithium and sodium adsorption properties. We have also evaluated its open circuit voltages (OCV). PLG revealed an excellent battery performance for Li and Na-ions and mixed-ion storage. These results highlight the PLG potential as a next-generation anode material for lithium and sodium-ion batteries, offering a unique combination of high storage capacity, efficient ion transport, and robust electrical conductivity.

\*Corresponding author  
ORCID(s):

## 2. Methodology

PLG structural, electronic, and lithium/sodium storage properties were investigated using DFT simulations with the CASTEP code [36]. All simulations employed the Perdew-Burke-Ernzerhof (PBE) exchange-correlation functional under the generalized gradient approximation (GGA) scheme [37]. A plane-wave energy cutoff of 450 eV and a Monkhorst-Pack  $\mathbf{k}$ -point mesh of  $10 \times 10 \times 1$  were used for the Brillouin zone sampling. Structural relaxations (atom positions and crystal lattice) were performed with periodic boundary conditions, ensuring minimal residual forces below  $10^{-3}$  eV/Å and pressure below 0.01 GPa. A vacuum buffer layer of 20 Å was applied along the out-of-plane direction to eliminate spurious mirror cell interactions. Van der Waals corrections were included within the Grimme D2 semi-empirical correction [38] to take into account dispersion effects.

Phonon calculations using density functional perturbation theory (DFPT) [39] confirmed the PLG dynamical stability. Additionally, *ab initio* molecular dynamics (AIMD) simulations were performed at 1000 K for 5 ps coupled to a Nosé-Hoover thermostat [40] in the NVT ensemble to assess thermal structural resilience, using a  $2 \times 2 \times 1$  supercell with a  $5 \times 5 \times 1$   $\mathbf{k}$ -points grid. These simulations were monitored for structural integrity, identifying potential bond-breaking regions, atomic reconfigurations, and structural failures.

The electronic band structure and density of states (DOS) were computed using  $\mathbf{k}$ -points grids of  $10 \times 10 \times 1$  and  $20 \times 20 \times 1$ , respectively. The metallic nature of X-Graphyne was verified through its band dispersion characteristics. Additionally, adsorption properties were investigated by placing Li and Na atoms at various randomly chosen adsorption sites and performing full geometry optimizations to determine the most stable configurations using the adsorption locator tool [41–43].

The adsorption energy ( $E_{\text{ads}}$ ) was calculated as:  $E_{\text{ads}} = E_{\text{X-Graphyne+M}} - (E_{\text{X-Graphyne}} + E_{\text{M}})$ , where  $E_{\text{X-Graphyne+M}}$  is the PLG total energy with an adsorbed ion ( $M = \text{Li}$  or  $\text{Na}$ ),  $E_{\text{X-Graphyne}}$  is the energy of pristine PLG, and  $E_{\text{M}}$  is the energy of an isolated metal ion. The nudged elastic band (NEB) method [44–46] was used to evaluate Li and Na diffusion barriers, providing insights into ion mobility across the surface.

## 3. Results

### 3.1. Structural and Mechanical Properties

First, we present the PLG structural characteristics. Fig. 1 illustrates the atomic structure of this novel material, which is composed of 4-, 8-, 10-, and 16-membered rings arranged in a periodic lattice. The unit cell (black box) comprises 40 carbon atoms and exhibits a porous topology. The symmetry group PM (CS-1) describes the material with an IT number of 6, reflecting its low symmetry and anisotropic atomic arrangement. The optimized unit cell parameters are  $a = 11.69$  Å and  $b = 11.68$  Å. PLG has

formation energy of  $-7.92$  eV, in the range value of other 2D carbon allotropes, which suggests thermodynamic stability.

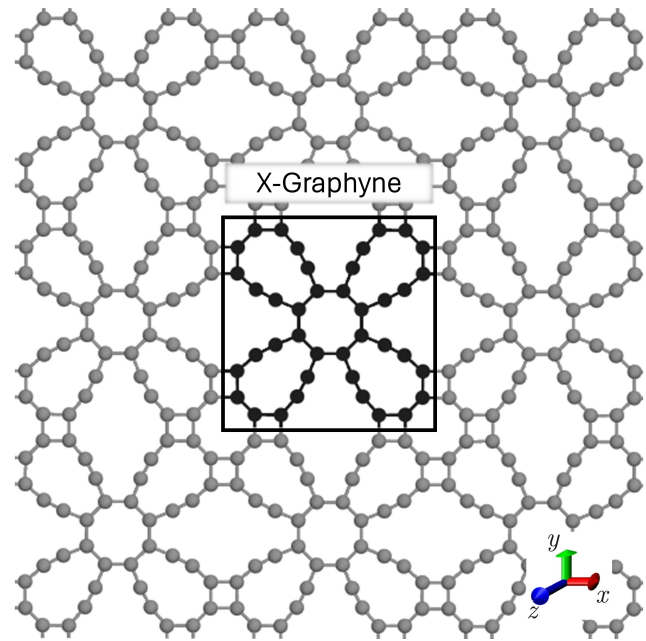


**Figure 1:** Atomic structure of petal-like graphyne (PLG). The black box highlights the structural unit cell, which contains 40 carbon atoms arranged in a porous framework with 4-, 8-, 10-, and 12-membered rings.

Phonon dispersion and AIMD simulations were performed to evaluate the PLG structural stability and AIMD), as shown in Fig. 2. The phonon dispersion is shown in Fig. 2(a) and confirms the PLG dynamical stability, as no imaginary frequencies are observed across the Brillouin zone. Three acoustic modes corresponding to longitudinal, transverse, and out-of-plane vibrations were also observed. Combining  $sp$  and  $sp^2$  hybridizations in the 2D lattice results in inhomogeneous bonding strengths. Regions with  $sp$ -hybridized bonds create local strain, stiffening specific vibrational modes, while  $sp^2$ -hybridized regions allow for softer modes at lower frequencies. This variation in bond strength leads to gaps in the phonon spectrum.

AIMD simulations carried out at 1000 K for 5 ps (Fig. 2(b)) confirm PLG thermal stability. The AIMD energy profile remains almost constant, indicating the absence of significant structural distortions or atomic reconstructions. The inset panels display the top and side views of the final AIMD snapshot, revealing that a planar-like structure is preserved even at high temperatures. No bond breaking or substantial out-of-plane deformations were observed, further confirming the PLG thermal robustness.

To better understand the PLG mechanical resilience, the evolution of bond lengths under different strain conditions was analyzed, as shown in Fig. 3. The subfigures 3(a), 3(b), and 3(c) illustrate the bond length variations as a function of the applied  $x$ -strain,  $y$ -strain, and  $xy$ -strain, respectively. Fig. 3(d) provides a structural representation of the key

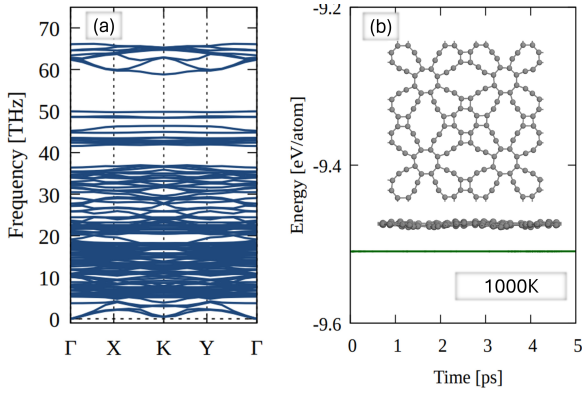


**Figure 2:** PLG stability analyses. (a) Phonon dispersion relation along high-symmetry points in the Brillouin zone and (b) AIMD simulation results at 1000 K over 5 ps. The inset panels display the structure's final top and side views at 5 ps.

bonds, with different colors indicating their behavior under deformation.

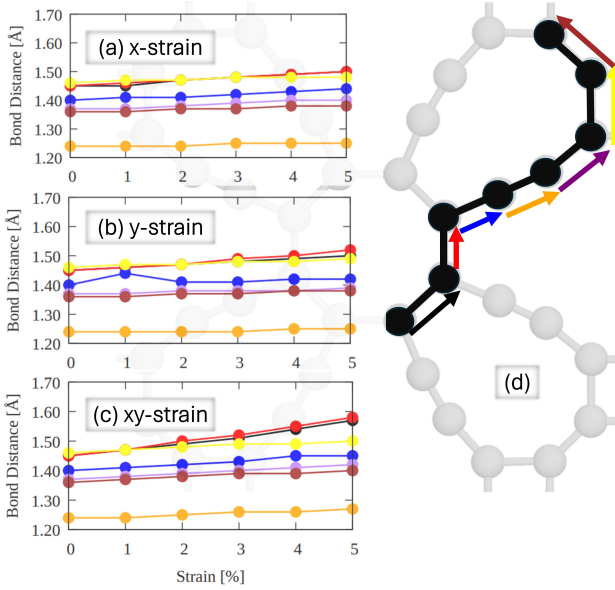


**Figure 3:** PLG bond length values evolution under applied strain. (a)  $x$ -strain, (b)  $y$ -strain, and (c)  $xy$ -strain show the variation in bond distances as a function of strain percentage, highlighting the anisotropic mechanical response. (d) Structural representation of the key bonds, with arrows indicating the primary deformation pathways under different strain conditions.

The bond length changes under strain exhibit an anisotropic behavior, which is expected given the PLG multi-ringed topology. Under  $x$ -strain (Fig. 3(a)), the bonds oriented along the stretching direction experience a gradual increase in length, while those perpendicular to it remain relatively unchanged. This feature indicates that PLG can accommodate stress by elongating specific bonds rather than uniformly distributing the strain. Similarly, under the  $y$ -strain (Fig. 3(b)), the bond length variations follow a similar trend

but with a distinct set of bonds experiencing elongation. The observed differences between  $x$ -strain and  $y$ -strain responses suggest directional-dependent mechanical properties, which could be important in practical applications requiring strain engineering.

When subjected to  $xy$ -strain (Fig. 3(c)), the bond deformation patterns become more complex due to shear stress interactions, leading to a more uniform increase in bond lengths across the different orientations. The structural representation in Fig. 3(d) further highlights how specific bonds stretch in different directions, with colored arrows indicating the primary deformation pathways. Both short and long bonds in the PLG framework result in a nontrivial stress redistribution, which may enhance its fracture resistance and mechanical flexibility.

The PLG mechanical properties were evaluated by calculating the directional Young's modulus  $Y(\theta)$  and Poisson's ratio  $\nu(\theta)$  values, as presented in Fig. 4. These quantities were obtained using the elastic constants and the equations presented below. The estimated elastic constants ( $C_{11} = 144.78$  N/m,  $C_{12} = 111.80$  N/m,  $C_{22} = 144.68$  N/m, and  $C_{66} = 61.64$  N/m) satisfy the Born–Huang mechanical stability criteria of the orthorhombic crystal ( $C_{11}C_{22} - C_{12}^2 > 0$  and  $C_{44} > 0$ ) [47, 48], confirming the PLG structural robustness. The Young's modulus  $Y(\theta)$  is given by:

$$Y(\theta) = \frac{C_{11}C_{22} - C_{12}^2}{C_{11} \sin^4 \theta + \left( \frac{C_{11}C_{22} - C_{12}^2 - 2C_{12}}{C_{66}} \right) \cos^2 \theta \sin^2 \theta + C_{22} \cos^4 \theta}, \quad (1)$$

and the Poisson's ratio  $\nu(\theta)$  is given by:

$$\nu(\theta) = \frac{C_{12}(\cos^4 \theta + \sin^4 \theta) - \left( \frac{C_{11} + C_{22} - \frac{C_{11}C_{22} - C_{12}^2}{C_{66}}}{C_{66}} \right) \cos^2 \theta \sin^2 \theta}{C_{11} \sin^4 \theta + \left( \frac{C_{11}C_{22} - C_{12}^2 - 2C_{12}}{C_{66}} \right) \cos^2 \theta \sin^2 \theta + C_{22} \cos^4 \theta}. \quad (2)$$

In Fig. 4, we can observe that the PLG calculated Young's modulus reaches a maximum value of approximately 180 N/m and a minimum one of around 60 N/m, highlighting its significant mechanical anisotropy. Compared to graphynes, which exhibit Young's modulus values ranging from 180 N/m to 220 N/m [49], PLG exhibits a lower overall stiffness due to its larger multi-membered rings that introduce additional structural flexibility. Similarly, compared with graphdiyne, which has a modulus of 100 N/m–150 N/m [50], PLG presents a comparable but slightly wider range of mechanical responses, indicating that its porous structure enhances flexibility while maintaining sufficient rigidity for structural stability.

The Poisson's ratio distribution is shown in Fig. 4(b), quantifying the material's lateral response to applied strain.

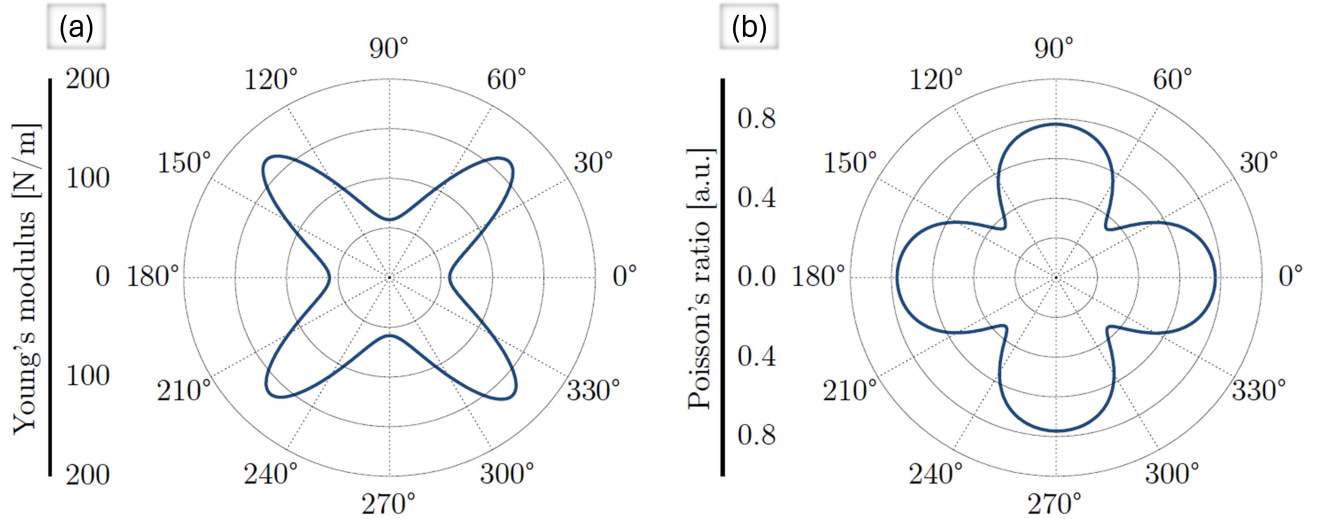


**Figure 4:** PLG anisotropic mechanical properties. (a) The polar plots of Young's modulus and (b) Poisson's ratio values.

The plot exhibits a fourfold symmetry, exhibiting the expected direction-dependent deformation behavior. The maximum Poisson's ratio reaches approximately 0.8, which is relatively high for 2D materials, while remaining strictly positive in all directions, confirming that PLG is not auxetic. Instead, the material follows the conventional Poisson effect, where stretching it along one direction leads to contraction in the perpendicular direction. The variation in Poisson's ratio across different orientations suggests that PLG undergoes non-uniform lateral deformation as the result of the multi-ring topology and anisotropic bonding environment.

### 3.2. Electronic and Optical Properties

In Fig. 5, we present the PLG electronic band structure 5(a), the corresponding projected density of states (PDOS) 5(b), the highest occupied crystalline orbital (HOCO) 5(c), the lowest unoccupied crystalline orbital (LUCO) 5(d), and the electron localization function 5(e).

Fig. 5(a) displays the PLG electronic band structure, confirming that it is metallic, as multiple bands cross the Fermi level (set at 0 eV). Unlike gamma-graphyne, which exhibits a semiconducting behavior with an electronic band gap in the range of 0.4 eV to 1.0 eV [51], and graphdiyne, which has a larger band gap of approximately 0.5–1.2 eV [52], PLG maintains a gapless electronic structure. The PLG metallicity is a direct consequence of its extended  $\pi$ -conjugation and multi-ring topology, where the delocalized electron network provides high electrical conductivity, a key feature for applications in energy storage and electronic devices.

The PDOS in Fig. 5(b) shows that the electronic states near the Fermi level are predominantly composed of  $2p_z$ -orbitals. This feature indicates that the  $\pi$ -electron network dominates its electronic properties. Importantly, this behavior is similar to that observed in graphyne and graphdiyne, where the  $sp^2$ -hybridized carbon atoms contribute significantly to the density of states. However, in PLG, the higher

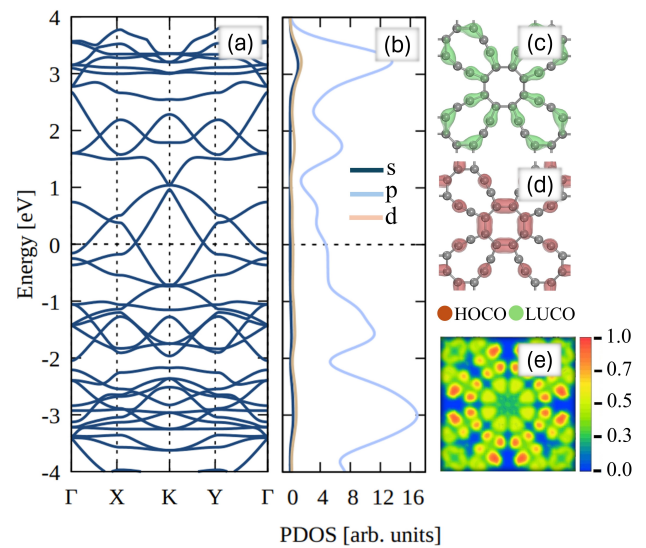


**Figure 5:** PLG electronic properties. (a) Electronic band structure, (b) Corresponding projected density of states (PDOS), (c) Highest occupied crystalline orbital (HOCO), (d) Lowest unoccupied crystalline orbital (LUCO), and (e) Electron localization function.

density of states at the Fermi level suggests an enhanced charge carrier concentration, making it a superior candidate for electronic transport applications compared to its semiconducting counterparts.

Figs. 5(c) and 5(d) show the HOCO and LUCO orbital distributions, respectively. The HOCO and LUCO contributions are widely distributed throughout the framework. This delocalization ensures efficient charge transport, which is beneficial for electrode materials in batteries and supercapacitors. In contrast, graphyne and graphdiyne often exhibit localized electronic states due to their larger ring sizes, which can limit carrier mobility [53–55].

The electron localization function (Fig. 5(e)) shows a uniform charge distribution throughout the structure, further reinforcing its metallic nature. The high electron density in the 10-membered ring indicates that charge carriers can move freely, enhancing the overall electrical conductivity. Again, this behavior differs from graphyne and graphdiyne [56, 57], where the electron density is often concentrated around specific bonds due to localized conjugation effects.

To investigate the PLG potential for optoelectronic applications, the optical absorption coefficient ( $\alpha$ ), reflectivity ( $R$ ), and refractive index ( $\eta$ ) as functions of photon energy were examined, as shown in Fig. 6.

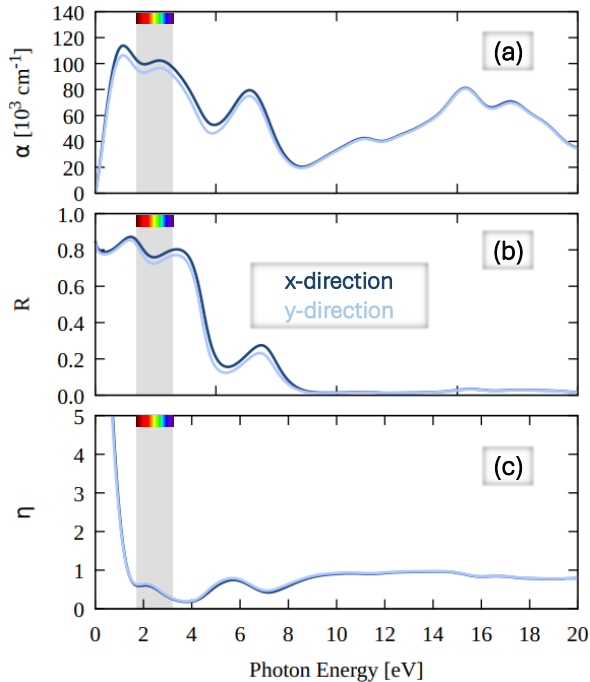


**Figure 6:** PLG optical properties as a function of photon energy. (a) Absorption coefficient ( $\alpha$ ), (b) reflectivity ( $R$ ) spectrum, and (c) refractive index ( $\eta$ ).

Fig. 6(a) shows the absorption coefficient  $\alpha$ . The absorption spectrum exhibits a strong and broad response, with activities in the infrared (IR), visible (VIS), and ultraviolet (UV) regions, with peaks also extending into these regions. PLG exhibits high absorption above 2 eV, indicating that it can interact efficiently with UV and visible light. Compared to graphyne and graphdiyne, which exhibit absorption edges around 1.5 eV–2.0 eV [58, 59], PLG presents a blue-shifted absorption profile, suggesting an enhanced optical response in higher-energy regions. The anisotropy between the  $x$ - and  $y$ -directions is slightly different, indicating nearly isotropic optical absorption.

The reflectivity spectrum ( $R$ ), which describes the fraction of incident light that is reflected by the material, is presented in Fig. 6(b). PLG exhibits a high reflectivity across the solar emission spectral range (0 eV to 4 eV), particularly in the visible region, making it an efficient light-reflecting material with reflectivity around 80%. The reflectivity sharply

drops after 3 eV. Compared to graphyne and graphdiyne, which exhibit moderate reflectivity variations [58–60], PLG shows a higher uniform and consistently high reflectivity in the infrared and visible regions of the electromagnetic spectrum.

Fig. 6(c) illustrates the refractive index ( $\eta$ ), which determines the phase velocity of light within the material. PLG exhibits a peak in the refractive index at low photon excitation energies, followed by a gradual decline, characteristic of materials with metallic behavior. This trend contrasts with semiconducting graphyne and graphdiyne, which display higher refractive indices in the visible range due to their band gap-related optical transitions [58–60].

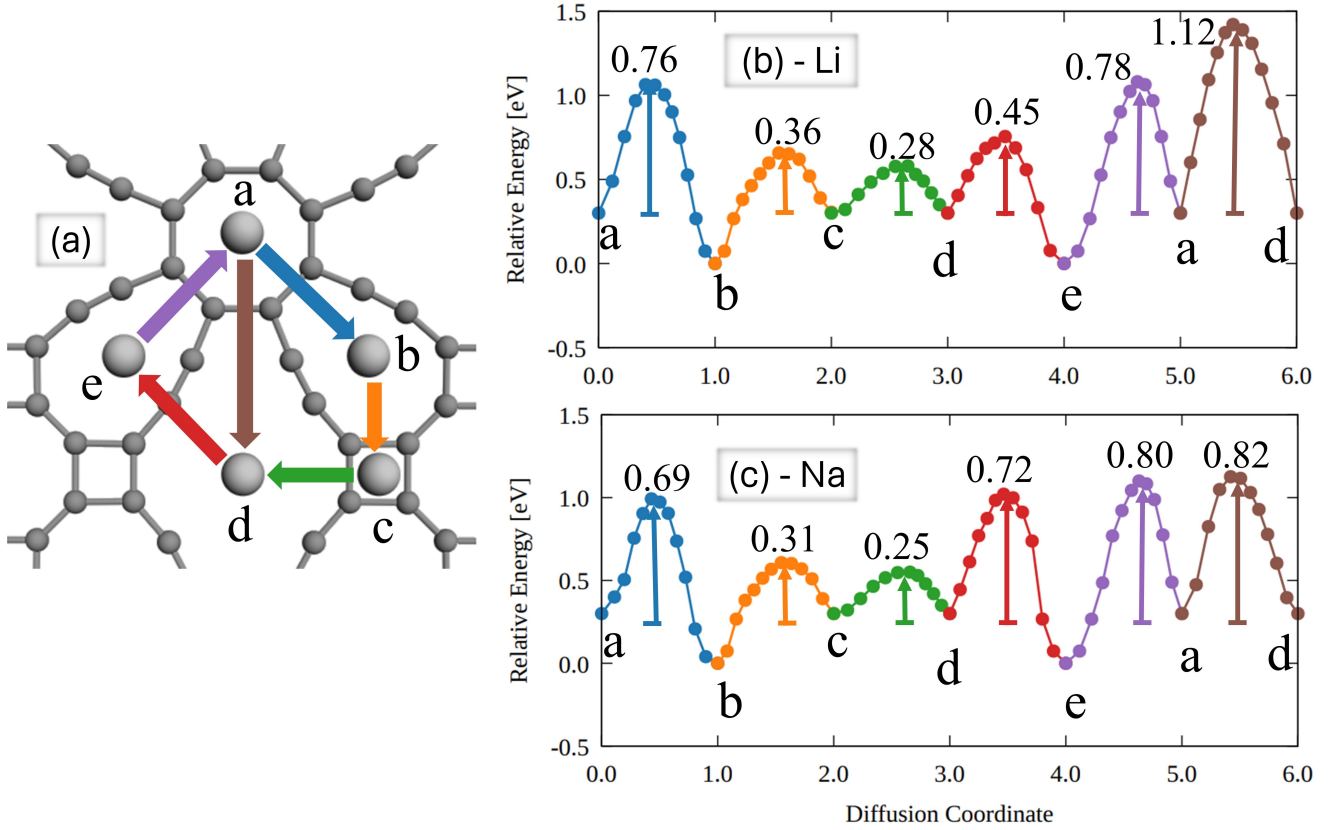
### 3.3. Li/Na-ion diffusion on monolayer and bilayer PLG

Fig. 7 shows the diffusion pathways and energy barriers for Li and Na ions analyzed and illustrated to evaluate PLG ion storage and transport capabilities. Diffusion behavior plays a crucial role in determining the efficiency of a material as an anode for lithium-ion batteries (LIBs) and sodium-ion batteries (SIBs). Low diffusion barriers lead to faster charge/discharge rates and improved electrochemical performance.

Fig. 7(a) presents possible diffusion pathways for Li and Na ions within the PLG lattice, highlighting key adsorption sites (a, b, c, d, and e) and their respective transition routes. The pathways span the multi-membered rings, allowing ion migration through interconnected pores in the structure. The diffusion energy profiles for Li and Na ions are shown in Fig. 7(b) and 7(c), respectively, where the relative energy barriers along different pathways are presented. For Li-ion diffusion (Fig. 7(b)), the lowest energy barrier is 0.28 eV, observed along the c–d path, while the highest barrier reaches 1.12 eV along the d–a transition. The moderate energy barriers in multiple pathways suggest that Li ions can efficiently migrate through the structure, though some transitions require additional energy input (energy-activated process).

For Na-ion diffusion (Fig. 7(c)), the lowest energy barrier is 0.25 eV, slightly lower than Li ions, indicating that Na ions can migrate with similar or improved mobility along specific paths. However, the highest Na diffusion barrier reaches 0.82 eV, which, although lower than the highest Li barrier, suggests that some migration pathways may still be limited. Even with distinct ion barriers, both Li and Na ions prefer to migrate across the 4-membered and 16-membered rings. The results suggest that PLG has comparable Li/Na ion migrations like other similar structures, such as graphyne (x/y eV), graphdiyne (x/y eV), irida-graphene (0.19/0.09 eV) [10, 11], Biphenylene (0.23/0.20 eV) [61, 62] and T-graphene (0.37/0.35 eV) [63].

To further analyze the PLG ionic transport properties, the diffusion coefficients for Li and Na ions as a function of temperature were calculated and presented in Fig. 8. The diffusion coefficient  $D_{\text{coeff}}(T)$  was determined using the Arrhenius-type equation:



**Figure 7:** PLG ion diffusion pathways and energy barriers. (a) Schematic representation of Li/Na diffusion paths between adsorption sites (a–e) within the porous PLG structure. (b) The diffusion energy profile for Li-ions shows the lowest energy barrier of 0.28 eV along the c–d path and the highest barrier of 1.12 eV along the d–a transition. (c) The diffusion energy profile for Na-ions has a minimum barrier of 0.25 eV and a maximum of 0.82 eV.

$$D_{\text{coeff}}(T) = L^2 \nu_0 \exp\left(-\frac{\Delta E_b}{k_B T}\right), \quad (3)$$

where  $\Delta E_b$  represents the diffusion barrier,  $L$  is the length of the diffusion path,  $T$  is the absolute temperature,  $\nu_0$  is the vibrational frequency (typically 10 THz), and  $k_B$  is the Boltzmann constant ( $8.62 \times 10^{-5}$  eV/K) [64].

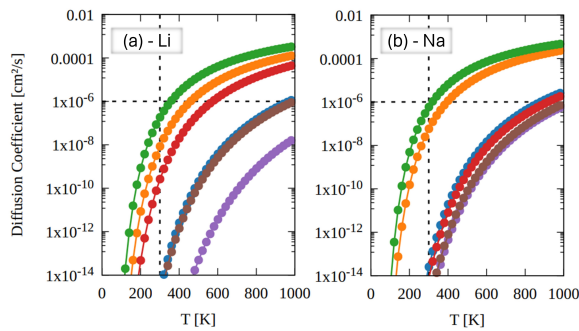


**Figure 8:** Temperature dependence of the diffusion coefficients for Li and Na ions. (a) Diffusion coefficient of Li ions and (b) diffusion coefficient of Na ions. The black dashed line refers to the graphene diffusion coefficient at room temperature.

Fig. 8(a) presents the diffusion coefficients for Li ions, while Fig. 8(b) shows the values for Na ions. At room temperature, Li exhibits a diffusion coefficient of approximately  $10^{-8}$  cm<sup>2</sup>/s, while Na shows a slightly lower value. As expected, both ions exhibit exponential increases in diffusion coefficients with increasing temperature, consistent with the Arrhenius relation. The black dashed line refers to the graphene diffusion coefficient at ambient conditions for comparison.

Comparing the results with graphyne and graphdiyne, PLG exhibits similar or slightly enhanced ionic mobility, particularly at higher temperatures [65–67]. The low diffusion barriers observed in specific pathways (Fig. 7) contribute to the improved transport properties. Thus, the PLG high diffusivity can efficiently support fast charge/discharge cycles, reinforcing its potential as a promising anode material for LIBs and SIBs.

To evaluate the feasibility of Li and Na ion migration across multiple PLG layers, the vertical diffusion pathway between two adjacent layers (bilayer) was analyzed, as illustrated in Fig. 9. Understanding interlayer diffusion is crucial for assessing the PLG viability as an anode material in stacked electrode configurations, which can enhance the energy storage capacity of battery systems.

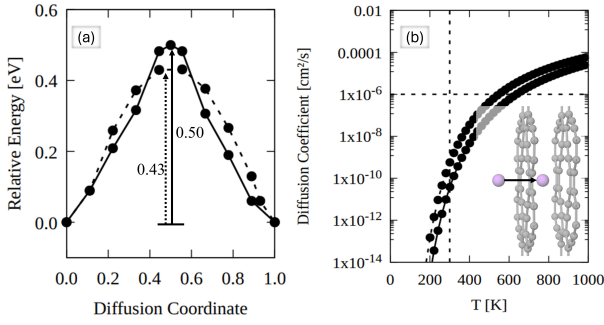


**Figure 9:** PLG interlayer diffusion of Li and Na ions. (a) Energy profile for ion migration between two adjacent PLG layers. (b) Temperature-dependent diffusion coefficient for interlayer migration. The inset illustrates the interlayer hopping mechanism, where ions move through the pores between two PLG layers.

Fig. 9(a) presents the diffusion energy profile for ion migration between two PLG layers. The calculated diffusion barrier for Li ions is approximately 0.50 eV, while for Na ions, it is 0.43 eV. These values indicate that interlayer diffusion is energetically feasible, albeit with slightly higher barriers than in-plane migration (Fig. 7). The higher interlayer barrier can be attributed to the van der Waals interactions between the PLG layers, which introduce additional resistance to ion movement.

The temperature-dependent diffusion coefficient for interlayer migration, calculated using the Arrhenius relation, is presented in Fig. 9(b). The inset illustrates the interlayer hopping mechanism, where ions move through the pores between two PLG layers. At room temperature, the diffusion coefficient for Li ions remains in the range of  $10^{-10}$  cm<sup>2</sup>/s, which is lower than the in-plane diffusion but still suitable for battery applications [68]. The inset schematic illustrates the interlayer hopping mechanism, where Li or Na ions move through the pores between two PLG layers. Compared to graphyne and graphdiyne, which typically exhibit higher interlayer barriers due to their denser frameworks [69], PLG presents a more accessible interlayer diffusion path, suggesting its potential for multilayer electrode architectures.

### 3.4. Storage Capacity and Open-circuit Voltage

Metal adsorption analyses were carried out to further assess the practical application of PLG as an anode material for LIBs and SIBs. Different adsorption sites on the PLG surface were systematically examined for single Li/Na adsorption. Our results indicate that the pore regions on the PLG lattice exhibit the highest stability for starting the lithiation/sodiation processes. Li and Na metals were selectively introduced to avoid clustering during charge/discharge cycles while ensuring appropriate Li-Li and Na-Na distances, as observed in the bulk phase. Consequently, the maximum metal loading is achieved when 18 Li and 18 Na atoms are adsorbed onto the PLG monolayer.

Fig. 10 illustrates the evolution of the adsorption energy ( $E_{\text{ads}}$ ) as a function of the number of Li, Na, and mixed

Li/Na atoms adsorbed on the PLG surface. This analysis provides important insights into the binding strength, stability, and maximum storage capacity of ions within the material, which are essential for its performance as a battery anode.

The adsorption energy remains negative in all cases, confirming that Li and Na adsorption is thermodynamically favorable across all studied concentrations, suggesting favorable electrochemical performance. This trend has also been observed in other graphyne-based lattices [70–72]. The adsorption energy curve exhibits a characteristic non-monotonic trend, where  $E_{\text{ads}}$  initially decreases as more atoms are added, reaching a minimum value and gradually increasing as saturation limit is reached.

For Li adsorption (Fig. 10(a)), the most energetically favorable configuration occurs at approximately 12 atoms, corresponding to the lowest value. Beyond this point, additional Li atoms experience weaker binding due to reduced available adsorption sites and repulsive interactions, leading to a progressive increase in adsorption energy. A similar trend is observed for Na adsorption (Fig. 10(b)), though Na exhibits slightly weaker binding than Li, as reflected in its higher minimum adsorption energy. This difference aligns with the larger ionic radius of Na, which affects its interaction with the PLG lattice.

The behavior of mixed Li/Na adsorption (Fig. 10(c)) closely follows the trends observed for individual species, with a balanced interaction between Li and Na atoms. The co-adsorption mechanism suggests that PLG can simultaneously accommodate Li and Na without significant clustering or structural instability, making it a promising candidate for dual-ion battery applications.

Another essential parameter for efficient battery performance is the OCV profile (see Fig. 11). Here, the OCV values were obtained using the expression:

$$\text{OCV} = \frac{E_{X\text{-Graphyne}} + N E_{\text{M}} - E_{N\text{-M+X-Graphyne}}}{N e} \quad (4)$$

where  $E_{X\text{-Graphyne}}$  is the total energy of pristine PLG,  $E_{\text{M}}$  represents the energy of a single metal atom (Li or Na), and  $E_{N\text{-M+X-Graphyne}}$  corresponds to the total energy of PLG with  $N$  adsorbed metal atoms. The parameter  $e$  denotes the elementary charge of an electron.

Figs. 11(a), 11(b), and 11(c) show the OCV evolution as a function of the number of Li, Na, and Li/Na adsorbed atoms. The OCV follows a stepwise decrease, which is expected due to the gradual occupation of adsorption sites and the corresponding change in interaction energies. The insets depict the fully adsorbed structures, where Li and Na atoms occupy positions above and below the PLG layer. At maximum metal loading, the OCV values are approximately 0.2 V for all the systems. As widely reported [73], the OCV should remain low and positive, typically below 1.0 V. Conversely, negative OCV values could lead to metal plating and result in battery failure. Regarding these features, PLG meets these requirements, ensuring stable and safe electrode performance.

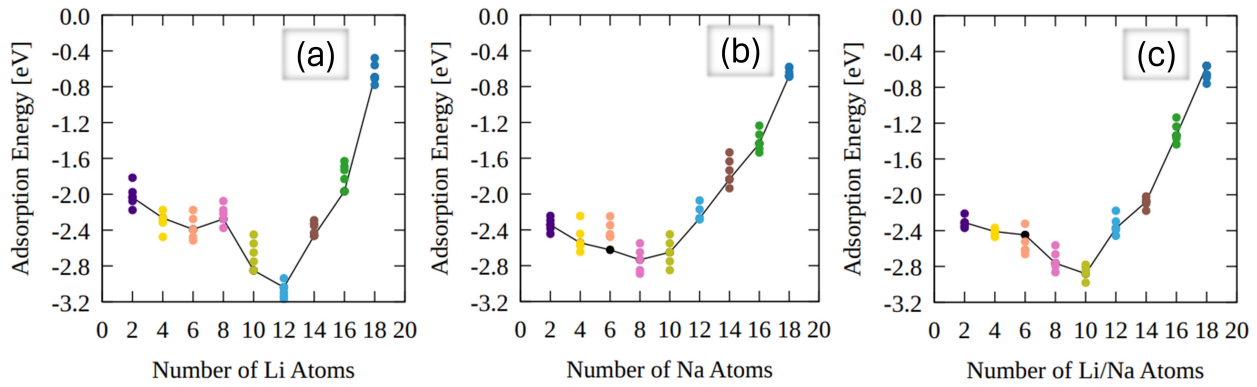


**Figure 10:** Evolution of adsorption energy as a function of the number of adsorbed ions on PCL monolayer. (a) The adsorption energy profile for Li atoms, (b) Na atoms, and (c) mixed Li/Na adsorption behavior.

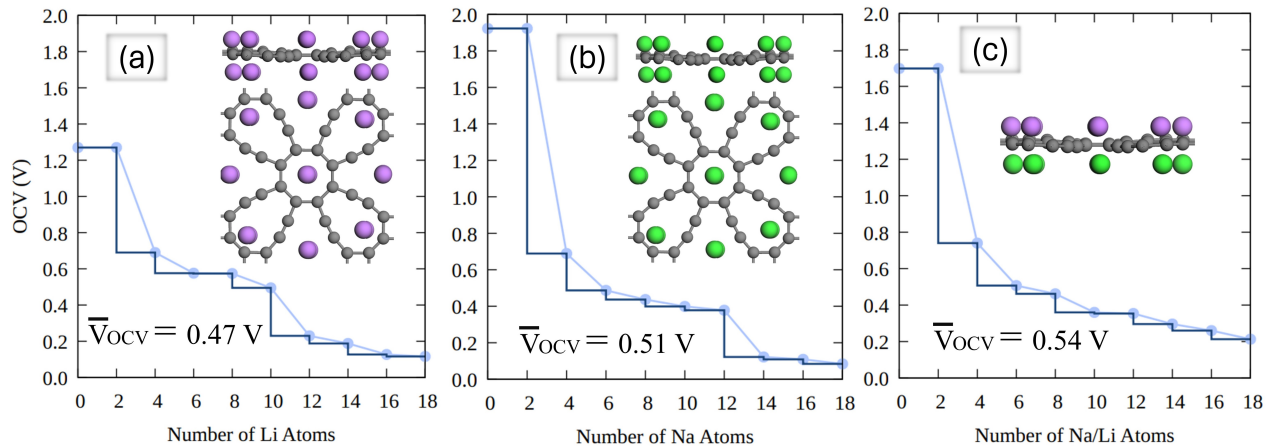


**Figure 11:** Open-circuit voltage (OCV) and Li and Na adsorption behavior in PLG. (a) OCV profile as a function of the number of adsorbed Li atoms, with an average OCV of 0.47 V. (b) OCV profile for Na adsorption, showing an average OCV of 0.51 V. (c) OCV profile for the mixed Li/Na system, with an average OCV of 0.54 V. Insets illustrate the fully adsorbed configurations, where Li (purple) and Na (green) atoms occupy positions above and below the PCL monolayer.

The thermal stability of fully lithiated and sodiated PLG is presented in Fig. ???. In this figure, the total energy per atom is monitored as a function of the simulation time, with the insets showing the final atomic configurations at the end of the AIMD simulations. In Fig. 12(a), the fully lithiated PLG system exhibits minimal energy fluctuations, with the total energy remaining nearly constant throughout the simulation. The final configuration confirms that Li atoms remain well-distributed over the surface without significant clustering and detachment, indicating structural stability and strong Li adsorption at the tested concentration values.

Similarly, Fig. 12(b) presents the AIMD results for the fully sodiated configuration. The system also maintains energetic stability over time, suggesting that Na adsorption does not induce substantial lattice distortions. However, compared to Li adsorption, Na exhibits slightly higher atomic displacements, likely due to its larger ionic radius and weaker binding energy, as previously observed in the adsorption energy analyses. Despite these minor displacements, no ion detachment was observed throughout the simulation, confirming the robustness of Na adsorption in

PLG. A similar trend is observed for the case considering the mixed Li/Na system (Fig. 12(c)). This configuration retains energetic stability comparable to the pure Li and Na cases, with no significant atomic reorganization or clustering. Importantly, all adsorbed ions remained anchored to the PLG surface, reinforcing the material's capability to sustain dual-ion storage without ion desorption or structural instability.

Finally, the PLG theoretical storage capacity ( $C$ ) was also evaluated by using the relation  $C = N_{MAX}F/M$ , where  $N_{MAX}$  is the maximum number of adsorbed Li/Na atoms,  $F$  is the Faraday constant (96 485.332 sA/mol), and  $M$  is the molar mass of the PLG supercell. Thus, the computed capacities are 1004 mAh/g for Li, Na, and mixed Li/Na ions, surpassing traditional graphite (372 mAh/g) [74, 75] and graphene anodes (744 mAh/g) [64, 74]. Theoretical capacities for PLG, as presented here, are not only competitive but, in some cases, surpass those of other graphyne-related materials for LIBs/SIBs, such as  $\gamma$ -Graphyne (1037/570 mAh/g),  $N$ -Graphdiyne (1660/623 mAh/g), penta-Graphyne (680/680 mAh/g), and Holey-Graphyne (873/558 mAh/g). In Table 3.4, we provide a compilation of these results



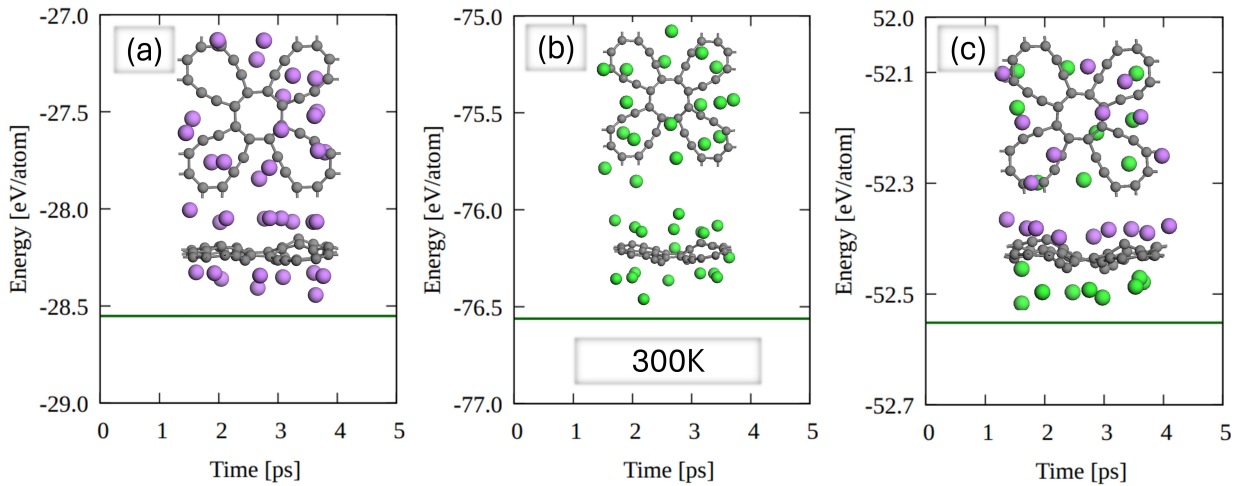


**Figure 12:** AIMD snapshots at 300 K for (a) fully lithiated, (b) sodiated, and (c) mixed Li/Na-PLG systems.

**Table 1**

Comparison of the storage capacity ( $C$ ) and in-plane energy barrier of PLG with other 2D materials used in LIBs and SIBs.

System	$C$ (mAh/g)	Energy barrier (eV)	Reference
Petal-Graphyne	1004/1004	0.28/0.25	this work
$\gamma$ -Graphyne	1037/570	0.44/0.46	[70]
$N$ -Graphdiyne	1660/623	0.80/0.79	[76]
Penta-Graphyne	680/680	0.49/0.61	[77]
Holey-Graphyne	873/558	0.28/0.32	[78]
Biphenylene	1302/1075	0.23/0.20	[61, 62]
Irida-graphene	1116/1022	0.19/0.09	[10, 11]
T-graphene	744/2232	0.37/0.35	[63]
$C_5N_2$	914/914	0.24/0.17	[9]

along with the corresponding energy barriers and data for other 2D carbon allotropes. These comparisons highlight the exceptional anodic performance of the PLG monolayer, particularly for Na-ion batteries.

## 4. Conclusions

In summary, the structural, electronic, mechanical, optical, and energy storage properties of Petal-Graphyne (PLG), a newly proposed 2D carbon allotrope, were investigated. This novel structure exhibits metallic behavior, with multiple band crossings at the Fermi level, ensuring high electrical conductivity for electrochemical applications. The phonon dispersion and AIMD simulations confirm its thermal and dynamical stability, while its anisotropic mechanical properties reveal a maximum and minimum Young's modulus of 180 N/m and 60 N/m, respectively.

The optical analyses highlights strong absorption in the ultraviolet region, high reflectivity, and a refractive index profile consistent with metallic materials, making PLG a good candidate for optoelectronic applications. Additionally, the material demonstrates a high theoretical energy storage capacity of 1004 mAh/g for both Li and Na-ions, outperforming conventional graphite, graphene, and other 2D carbon-based anodes. The average OCV values of 0.47 V

(Li), 0.51 V (Na), and 0.54 V (Li/Na) indicates stable electrochemical performance. The lowest in-plane diffusion barriers of 0.28 eV (Li) and 0.25 eV (Na) suggest good ion mobility, while the interlayer diffusion barriers of 0.50 eV (Li) and 0.43 eV (Na) confirm viable transport in stacked configurations.

## Data access statement

Data supporting the results can be accessed by contacting the corresponding author.

## Conflicts of interest

The authors declares no conflict of interest.

## Acknowledgements

This work was supported by the Brazilian funding agencies Fundação de Amparo à Pesquisa do Estado de São Paulo - FAPESP (grant no. 2022/03959-6, 2022/00349- 2, 2022/14576-0, 2020/01144-0, 2024/05087-1, and 2022/16509-9), and National Council for Scientific, Technological Development - CNPq (grant no. 307213/2021-8). L.A.R.J. acknowledges the financial support from FAP-DF grants

00193.00001808/2022-71 and 00193-00001857/2023-95, FAPDF-PRONEM grant 00193.00001247/2021-20, PDPG-FAPDF-CAPEs Centro-Oeste 00193-00000867/2024-94, and CNPq grants 350176/2022 – 1 and 167745/2023 – 9. A.C.D acknowledges the following FAP-DF grants: 00193-00001817/2023-43 and 00193-00002073/2023-84, the following CNPq grants: 408144/2022-0, 305174/2023-1, 444069/2024-0 and 444431/2024-1, and the computational resources from Cenapad-SP (project 897) and Lobo Carneiro HPC (project 133). K.A.L.L. and D.S.G. acknowledge the Center for Computational Engineering & Sciences (CCES) at Unicamp for financial support through the FAPESP/CEPID Grant 2013/08293-7.

## CRedit authorship contribution statement

**Kleuton A. L. Lima:** Conceptualization of this study, Methodology, Review and editing, Investigation, Formal analysis, Writing – review & editing, Writing – original draft. **José A. S. Laranjeira:** Conceptualization of this study, Methodology, Review and editing, Investigation, Formal analysis, Writing – review & editing, Writing – original draft. **Nicolas F. Martins:** Conceptualization of this study, Methodology, Review and editing, Investigation, Formal analysis, Writing – review & editing, Writing – original draft. **Alexandre C. Dias:** Conceptualization of this study, Methodology, Review and editing, Investigation, Formal analysis, Writing – review & editing, Writing – original draft. **Julio R. Sambrano:** Conceptualization of this study, Methodology, Review and editing, Investigation, Formal analysis, Writing – review & editing, Writing – original draft. **Douglas S. Galvão:** Conceptualization of this study, Methodology, Review and editing, Investigation, Formal analysis, Writing – review & editing, Writing – original draft. **Luiz A. Ribeiro Junior:** Conceptualization of this study, Methodology, Review and editing, Investigation, Formal analysis, Writing – review & editing, Writing – original draft.

## References

- [1] Santosh K Tiwari, Vijay Kumar, Andrzej Huczko, R Oraon, A De Adhikari, and GC Nayak. Magical allotropes of carbon: prospects and applications. *Critical Reviews in Solid State and Materials Sciences*, 41(4):257–317, 2016.
- [2] Salisu Nasir, Mohd Zobir Hussein, Zulkarnain Zainal, and Nor Azah Yusof. Carbon-based nanomaterials/allotropes: A glimpse of their synthesis, properties and some applications. *Materials*, 11(2):295, 2018.
- [3] Andreas Hirsch. The era of carbon allotropes. *Nature materials*, 9(11):868–871, 2010.
- [4] Wen-cai Yi, Wei Liu, Jorge Botana, Jing-yao Liu, and Mao-sheng Miao. Microporosity as a new property control factor in graphene-like 2d allotropes. *Journal of Materials Chemistry A*, 6(22):10348–10353, 2018.
- [5] Xiaoyu Zheng, Jiayan Luo, Wei Lv, Da-Wei Wang, and Quan-Hong Yang. Two-dimensional porous carbon: synthesis and ion-transport properties. *Advanced Materials*, 27(36):5388–5395, 2015.
- [6] Rajib Paul, Mewin Vincent, Vinodkumar Etacheri, and Ajit K Roy. Carbon nanotubes, graphene, porous carbon, and hybrid carbon-based materials: synthesis, properties, and functionalization for efficient energy storage. In *Carbon Based Nanomaterials for Advanced Thermal and Electrochemical Energy Storage and Conversion*, pages 1–24. Elsevier, 2019.
- [7] Tongtong Li, Cheng He, and Wenxue Zhang. Rational design of porous carbon allotropes as anchoring materials for lithium sulfur batteries. *Journal of Energy Chemistry*, 52:121–129, 2021.
- [8] K.A.L. Lima, D.A. da Silva, G.D. Amvame Nze, F.L. Lopes de Mendonça, M.L. Pereira, and L.A. Ribeiro. Structural, electronic, and li-ion adsorption properties of polypygy explored by first-principles and machine learning simulations: A new multi-ringed 2d carbon allotrope. *Journal of Energy Storage*, 117:116099, 2025.
- [9] Manqi You, Gencai Guo, Yujie Liao, Siwei Luo, Chaoyu He, Chao Tang, and Jianxin Zhong. 2d novel c5n2 allotropes: High-performance anode materials for alkali metal ion battery. *Journal of Energy Storage*, 84:111004, 2024.
- [10] Xin Xiong, Hong-Bao Cao, Zheng Lu, Chun-Sheng Liu, and Xiao-Juan Ye. Theoretical prediction on irida-graphene monolayer as promising anode material for lithium-ion batteries. *Computational Materials Science*, 244:113225, 2024.
- [11] Nicolas F Martins, José A Laranjeira, Guilherme SL Fabris, Pablo A Denis, and Julio R Sambrano. Irida-graphene as a high-performance anode for sodium batteries. *Journal of Energy Storage*, 104:114637, 2024.
- [12] Andre K Geim and Konstantin S Novoselov. The rise of graphene. *Nature materials*, 6(3):183–191, 2007.
- [13] Victor G Desyatkin, William B Martin, Ali E Aliev, Nathaniel E Chapman, Alexandre F Fonseca, Douglas S Galvão, Ericka Roy Miller, Kevin H Stone, Zhong Wang, Dante Zakhidov, et al. Scalable synthesis and characterization of multilayer  $\gamma$ -graphyne, new carbon crystals with a small direct band gap. *Journal of the American Chemical Society*, 144(39):17999–18008, 2022.
- [14] Qitang Fan, Linghao Yan, Matthias W Tripp, Ondřej Krejčí, Stavrina Dimosthenous, Stefan R Kachel, Mengyi Chen, Adam S Foster, Ulrich Koert, Peter Liljeroth, et al. Biphenylene network: A nonbenzenoid carbon allotrope. *Science*, 372(6544):852–856, 2021.
- [15] Lingxiang Hou, Xueping Cui, Bo Guan, Shaozhi Wang, Ruian Li, Yunqi Liu, Daoben Zhu, and Jian Zheng. Synthesis of a monolayer fullerene network. *Nature*, 606(7914):507–510, 2022.
- [16] Mathew A Hudspeth, Brandon W Whitman, Veronica Barone, and Juan E Peralta. Electronic properties of the biphenylene sheet and its one-dimensional derivatives. *ACS nano*, 4(8):4565–4570, 2010.
- [17] Savas Berber, Eiji Osawa, and David Tománek. Rigid crystalline phases of polymerized fullerenes. *Physical Review B—Condensed Matter and Materials Physics*, 70(8):085417, 2004.
- [18] RH Baughman, H Eckhardt, and M Kertesz. Structure-property predictions for new planar forms of carbon: Layered phases containing sp<sup>2</sup> and sp atoms. *The Journal of chemical physics*, 87(11):6687–6699, 1987.
- [19] Philip Richard Wallace. The band theory of graphite. *Physical review*, 71(9):622, 1947.
- [20] Shunhong Zhang, Jian Zhou, Qian Wang, Xiaoshuang Chen, Yoshiyuki Kawazoe, and Puru Jena. Penta-graphene: A new carbon allotrope. *Proceedings of the National Academy of Sciences*, 112(8):2372–2377, 2015.
- [21] Shuaiwei Wang, Baocheng Yang, Houyang Chen, and Eli Ruckenstein. Popgraphene: a new 2d planar carbon allotrope composed of 5–8–5 carbon rings for high-performance lithium-ion battery anodes from bottom-up programming. *Journal of Materials Chemistry A*, 6(16):6815–6821, 2018.
- [22] Zhenhai Wang, Xiang-Feng Zhou, Xiaoming Zhang, Qiang Zhu, Huafeng Dong, Mingwen Zhao, and Artem R Oganov. Phagraphene: a low-energy graphene allotrope composed of 5–6–7 carbon rings with distorted dirac cones. *Nano letters*, 15(9):6182–6186, 2015.
- [23] ML Pereira Júnior, Wiliam Ferreira da Cunha, William Ferreira Giozza, Rafael Timoteo de Sousa Junior, and LA Ribeiro Junior. Irida-graphene: A new 2d carbon allotrope. *FlatChem*, 37:100469, 2023.
- [24] Raphael M Tromer, Marcelo L Pereira Junior, Kleuton A L. Lima, Alexandre F Fonseca, Luciano R da Silva, Douglas S Galvão, and

- Luiz A Ribeiro Junior. Mechanical, electronic, and optical properties of 8-16-4 graphyne: A 2d carbon allotrope with dirac cones. *The Journal of Physical Chemistry C*, 127(25):12226–12234, 2023.
- [25] Xianwen Mao, Gregory C Rutledge, and T Alan Hatton. Nanocarbon-based electrochemical systems for sensing, electrocatalysis, and energy storage. *Nano Today*, 9(4):405–432, 2014.
- [26] Xin-Wei Chen, Zheng-Zhe Lin, and Xi-Mei Li. Biphenylene network as sodium ion battery anode material. *Physical Chemistry Chemical Physics*, 25(5):4340–4348, 2023.
- [27] David Ferguson, Debra J Searles, and Marlies Hankel. Biphenylene and phagraphene as lithium ion battery anode materials. *ACS applied materials & interfaces*, 9(24):20577–20584, 2017.
- [28] EAJ Santos, KAL Lima, and LA Ribeiro Junior. Proposing todd-graphene as a novel porous 2d carbon allotrope designed for superior lithium-ion battery efficiency. *Scientific Reports*, 14(1):6202, 2024.
- [29] Saif Ullah, Marcos G Menezes, and Alexander M Silva. Theoretical characterization of tolanene: A new 2d sp-sp<sup>2</sup> hybridized carbon allotrope. *Carbon*, 217:118618, 2024.
- [30] Juan Gomez Quispe, Bruno Ipaves, Douglas Soares Galvao, and Pedro Alves da Silva Autreto. Tpdh-graphene as a new anodic material for lithium ion battery: Dft-based investigations. *ACS omega*, 9(37):39195–39201, 2024.
- [31] Huili Liu, Yaru Wei, Donghai Wu, and Shuaiwei Wang. A novel 2d carbon allotrope for high-performance metal-ion battery anode material. *Materials Science in Semiconductor Processing*, 173:108146, 2024.
- [32] Tian-Kai Li, Xiao-Juan Ye, Lan Meng, and Chun-Sheng Liu. Thfs-carbon: a theoretical prediction of metallic carbon allotrope with half-auxeticity, planar tetracoordinate carbon, and potential application as anode for sodium-ion batteries. *Physical Chemistry Chemical Physics*, 25(22):15295–15301, 2023.
- [33] Zishuang Cheng, Xiaoming Zhang, Hui Zhang, Jianbo Gao, Heyan Liu, Xiao Yu, Xuefang Dai, Guodong Liu, and Guifeng Chen. Two-dimensional metallic carbon allotrope with multiple rings for ion batteries. *Physical Chemistry Chemical Physics*, 23(34):18770–18776, 2021.
- [34] Xiaoyin Li, Qian Wang, and Puru Jena.  $\psi$ -graphene: a new metallic allotrope of planar carbon with potential applications as anode materials for lithium-ion batteries. *The journal of physical chemistry letters*, 8(14):3234–3241, 2017.
- [35] Luye Sun, Wei Zheng, Faming Kang, Wenzhe Gao, Tongde Wang, Guohua Gao, and Wei Xu. On-surface synthesis and characterization of anti-aromatic cyclo [12] carbon and cyclo [20] carbon. *Nature Communications*, 15(1):7649, 2024.
- [36] Stewart J Clark, Matthew D Segall, Chris J Pickard, Phil J Hasnip, Matt IJ Probert, Keith Refson, and Mike C Payne. First principles methods using castep. *Zeitschrift für kristallographie-crystalline materials*, 220(5-6):567–570, 2005.
- [37] John P Perdew, Kieron Burke, and Matthias Ernzerhof. Generalized gradient approximation made simple. *Physical review letters*, 77:3865, 1996.
- [38] Stefan Grimme. Semiempirical gga-type density functional constructed with a long-range dispersion correction. *Journal of computational chemistry*, 27(15):1787–1799, 2006.
- [39] Stefano Baroni, Stefano De Gironcoli, Andrea Dal Corso, and Paolo Giannozzi. Phonons and related crystal properties from density-functional perturbation theory. *Reviews of modern Physics*, 73(2):515, 2001.
- [40] Shuichi Nosé. A unified formulation of the constant temperature molecular dynamics methods. *The Journal of chemical physics*, 81:511–519, 1984.
- [41] Nicholas Metropolis, Arianna W Rosenbluth, Marshall N Rosenbluth, Augusta H Teller, and Edward Teller. Equation of state calculations by fast computing machines. *The journal of chemical physics*, 21(6):1087–1092, 1953.
- [42] Scott Kirkpatrick, C Daniel Gelatt Jr, and Mario P Vecchi. Optimization by simulated annealing. *science*, 220(4598):671–680, 1983.
- [43] Vladimír Černý. Thermodynamical approach to the traveling salesman problem: An efficient simulation algorithm. *Journal of optimization theory and applications*, 45:41–51, 1985.
- [44] Stela Makri, Christoph Ortner, and James R Kermode. A preconditioning scheme for minimum energy path finding methods. *The Journal of Chemical Physics*, 150(9):094109, 2019.
- [45] Jonathan Barzilai and Jonathan M Borwein. Two-point step size gradient methods. *IMA journal of numerical analysis*, 8(1):141–148, 1988.
- [46] Erik Bitzek, Pekka Koskinen, Franz Gähler, Michael Moseler, and Peter Gumbsch. Structural relaxation made simple. *Physical review letters*, 97(17):170201, 2006.
- [47] Félix Mouhat and François-Xavier Coudert. Necessary and sufficient elastic stability conditions in various crystal systems. *Phys. Rev. B*, 90:224104, Dec 2014.
- [48] Yiran Ying, Ke Fan, Sicong Zhu, Xin Luo, and Haitao Huang. Theoretical investigation of monolayer rhtecl semiconductors as photocatalysts for water splitting. *The Journal of Physical Chemistry C*, 124(1):639–646, 2020.
- [49] Tianjiao Shao, Bin Wen, Roderick Melnik, Shan Yao, Yoshiyuki Kawazoe, and Yongjun Tian. Temperature dependent elastic constants and ultimate strength of graphene and graphyne. *The Journal of chemical physics*, 137(19), 2012.
- [50] Yang Pei. Mechanical properties of graphdiyne sheet. *Physica B: Condensed Matter*, 407(22):4436–4439, 2012.
- [51] Ali E Aliev, Yongzhe Guo, Alexandre F Fonseca, Joselito M Razal, Zhong Wang, Douglas S Galvão, Claire M Bolding, Nathaniel E Chapman-Wilson, Victor G Desyatkin, Johannes E Leisen, et al. A planar-sheet nongraphitic zero-bandgap sp<sup>2</sup> carbon phase made by the low-temperature reaction of  $\gamma$ -graphyne. *Proceedings of the National Academy of Sciences*, 122(5):e2413194122, 2025.
- [52] Jahyun Koo, Minwoo Park, Seunghyun Hwang, Bing Huang, Byungryul Jang, Yongkyung Kwon, and Hoonyung Lee. Widely tunable band gaps of graphdiyne: an ab initio study. *Physical Chemistry Chemical Physics*, 16(19):8935–8939, 2014.
- [53] Mengqiu Long, Ling Tang, Dong Wang, Yuliang Li, and Zhigang Shuai. Electronic structure and carrier mobility in graphdiyne sheet and nanoribbons: theoretical predictions. *ACS nano*, 5(4):2593–2600, 2011.
- [54] Linwei Li, Weiye Qiao, Hongcun Bai, and Yuanhe Huang. Structural and electronic properties of  $\alpha$ -,  $\beta$ -,  $\gamma$ -, and 6, 6, 18-graphdiyne sheets and nanotubes. *RSC advances*, 10(28):16709–16717, 2020.
- [55] Jiaqiang Li and Yu Han. Artificial carbon allotrope  $\gamma$ -graphyne: Synthesis, properties, and applications. *Giant*, 13:100140, 2023.
- [56] Xianwei Sha and Clifford M Krowne. First principles quantum calculations for graphyne for electronic devices. *Nanoscale Advances*, 3(20):5853–5859, 2021.
- [57] İskender Muz and Mustafa Kurban. The electronic structure, transport and structural properties of nitrogen-decorated graphdiyne nanomaterials. *Journal of Alloys and Compounds*, 842:155983, 2020.
- [58] Xun Hou, Zhongjing Xie, Chunmei Li, Guannan Li, and Zhiqian Chen. Study of electronic structure, thermal conductivity, elastic and optical properties of  $\alpha$ ,  $\beta$ ,  $\gamma$ -graphyne. *Materials*, 11(2):188, 2018.
- [59] Chuannan Ge, Jie Chen, Shaolong Tang, Youwei Du, and Nujiang Tang. Review of the electronic, optical, and magnetic properties of graphdiyne: from theories to experiments. *ACS applied materials & interfaces*, 11(3):2707–2716, 2018.
- [60] Hamed Jafarzadeh, Saeed Zahedi, and Amir Hossein Bayani. Electronic and optical properties of 14, 14, 18 graphyne as an anti-visible ray coating. *Optik*, 203:163905, 2020.
- [61] Nidhi Duhan, Brahmananda Chakraborty, and TJ Dhillip Kumar. 2-dimensional biphenylene monolayer as anode in li ion secondary battery with high storage capacity: Acumen from density functional theory. *Applied Surface Science*, 629:157171, 2023.
- [62] Ting Han, Yu Liu, Xiaodong Lv, and Fengyu Li. Biphenylene monolayer: a novel nonbenzenoid carbon allotrope with potential application as an anode material for high-performance sodium-ion

- batteries. *Physical Chemistry Chemical Physics*, 24(18):10712–10716, 2022.
- [63] Junping Hu, Yu Liu, Ning Liu, Jianwen Li, and Chuying Ouyang. Theoretical prediction of t-graphene as a promising alkali-ion battery anode offering ultrahigh capacity. *Physical Chemistry Chemical Physics*, 22(6):3281–3289, 2020.
- [64] Shuli Gao, Elyas Abduryim, Changcheng Chen, Chao Dong, Xiaoning Guan, Shuangna Guo, Yue Kuai, Ge Wu, Wen Chen, and Pengfei Lu. Twin-graphene: a promising anode material for lithium-ion batteries with ultrahigh specific capacity. *The Journal of Physical Chemistry C*, 127:14065–14074, 2023.
- [65] Hongyu Zhang, Yueyuan Xia, Hongxia Bu, Xiaopeng Wang, Meng Zhang, Youhua Luo, and Mingwen Zhao. Graphdiyne: A promising anode material for lithium ion batteries with high capacity and rate capability. *Journal of Applied Physics*, 113(4), 2013.
- [66] Massimiliano Bartolomei and Giacomo Giorgi. Sodium into  $\gamma$ -graphyne multilayers: An intercalation compound for anodes in metal-ion batteries. *ACS materials letters*, 6(10):4682–4689, 2024.
- [67] Mohammed Lemaalem, Nabil Khossossi, Gaelle Bouder, Poulumi Dey, and Philippe Carbonnière. Graphyne-based membrane as a promising candidate for li-battery electrodes protection: Insight from atomistic simulations. *Journal of Power Sources*, 581:233482, 2023.
- [68] Hyobin Lee, Seungwon Yang, Suhwan Kim, Jihun Song, Joonam Park, Chil-Hoon Doh, Yoon-Cheol Ha, Tae-Soon Kwon, and Yong Min Lee. Understanding the effects of diffusion coefficient and exchange current density on the electrochemical model of lithium-ion batteries. *Current Opinion in Electrochemistry*, 34:100986, 2022.
- [69] Yongjun Li, Liang Xu, Huibiao Liu, and Yuliang Li. Graphdiyne and graphyne: from theoretical predictions to practical construction. *Chemical Society Reviews*, 43(8):2572–2586, 2014.
- [70] Chaofan Yang, Chong Qiao, Yang Chen, Xueqi Zhao, Lulu Wu, Yong Li, Yu Jia, Songyou Wang, and Xiaoli Cui. Nitrogen doped  $\gamma$ -graphyne: A novel anode for high-capacity rechargeable alkali-ion batteries. *Small*, 16(10):1907365, 2020.
- [71] Tavinder Singh, Jyoti Roy Choudhuri, and Malay Kumar Rana.  $\alpha$ -graphyne as a promising anode material for na-ion batteries: a first-principles study. *Nanotechnology*, 34(4):045404, 2022.
- [72] Mokhtar Nasrollahpour, Mohsen Vafaei, Mohammad Reza Hosseini, and Hossein Iravani. Ab initio study of sodium diffusion and adsorption on boron-doped graphyne as promising anode material in sodium-ion batteries. *Physical Chemistry Chemical Physics*, 20(47):29889–29895, 2018.
- [73] Xiuying Zhang, Chen Yang, Yuanyuan Pan, Mouyi Weng, Linqiang Xu, Shiqi Liu, Jie Yang, Jiahuan Yan, Jingzhen Li, Bowen Shi, et al. Monolayer gas with high ion mobility and capacity as a promising anode battery material. *Journal of Materials Chemistry A*, 7(23):14042–14050, 2019.
- [74] Xiaoping Yi, Guoqing Qi, Xunliang Liu, Christopher Depcik, and Lin Liu. Challenges and strategies toward anode materials with different lithium storage mechanisms for rechargeable lithium batteries. *Journal of Energy Storage*, 95:112480, 2024.
- [75] Jakob Asenbauer, Tobias Eisenmann, Matthias Kuenzel, Arefeh Kazzazi, Zhen Chen, and Dominic Bresser. The success story of graphite as a lithium-ion anode material—fundamentals, remaining challenges, and recent developments including silicon (oxide) composites. *Sustainable Energy & Fuels*, 4(11):5387–5416, 2020.
- [76] Meysam Makaremi, Bohayra Mortazavi, Timon Rabczuk, Geofrey A Ozin, and Chandra Veer Singh. Theoretical investigation: 2d n-graphdiyne nanosheets as promising anode materials for li/na rechargeable storage devices. *ACS Applied Nano Materials*, 2(1):127–135, 2018.
- [77] Jyotirmoy Deb, Rajeev Ahuja, and Utpal Sarkar. Two-dimensional pentagraphyne as a high-performance anode material for li/na-ion rechargeable batteries. *ACS Applied Nano Materials*, 5(8):10572–10582, 2022.
- [78] Muhammad Sajjad, Khaled Badawy, J Andreas Larsson, Rehan Umer, and Nirpendra Singh. Two dimensional holey graphyne: An excellent anode and anchoring material for metal–ion and metal–sulfur batteries. *Carbon*, 214:118340, 2023.